

# Green synthesis of magnetic mesoporous silica nanocomposite and its adsorptive performance against organochlorine pesticides

W. A. El-Said<sup>1</sup> · D. M. Fouad<sup>1</sup> · M. H. Ali<sup>1</sup> · M. A. El-Gahami<sup>1</sup>

Received: 30 December 2016/Revised: 31 July 2017/Accepted: 5 September 2017/Published online: 13 September 2017  
© Islamic Azad University (IAU) 2017

**Abstract** Green synthesis of nanomaterials has received increasing attention as an eco-friendly technology in materials science. Here, we have used two types of extractions from green tea leaf (i.e., total extraction and tannin extraction) as reducing agents for a rapid, simple and one-step synthesis method of mesoporous silica nanoparticles/iron oxide nanocomposite based on deposition of iron oxide onto mesoporous silica nanoparticles. Mesoporous silica nanoparticles/iron oxide nanocomposite were characterized by X-ray diffraction, Fourier transform infrared spectroscopy, scanning electron microscopy, energy-dispersive X-ray, vibrating sample magnetometer, N<sub>2</sub> adsorption and high-resolution transmission electron microscopy. Mesoporous silica nanoparticles/iron oxide nanocomposite was used as a solid adsorbent for removal of lindane pesticide from aqueous solutions. The developed system possesses the advantages of silica as core that include large surface area and advantages of iron oxide (shell) that include the capability to interact with chlorinated compounds and ability to release by using external magnetic field. UV-Vis technique was used as a simple and easy method for monitoring the removal of lindane. Effects of pH and temperature on the removal efficiency of the developed mesoporous silica nanoparticles/iron oxide nanocomposite toward lindane pesticide were also investigated. Fourier transform infrared spectroscopy, high-performance liquid chromatography and gas

chromatography techniques were used to confirm the high ability of mesoporous silica nanoparticles/iron oxide nanocomposite for sensing and the capture of lindane molecules with high sorption capacity (about 99%) that could develop a new eco-friendly strategy for detection and removal of pesticide and as a promising material for water treatment.

**Keywords** Green synthesis · Mesoporous silica · Magnetic iron oxide nanoparticles · Adsorption · Lindane

## Introduction

Magnetic nanoparticles (NPs) have wide applications in several fields such as medical applications (e.g., target drug delivery, magnetic resonance imaging, cancer hyperthermia treatment) and nano-sorbents in environmental engineering (Johannsen et al. 2007). Several techniques have been used for the synthesis of iron oxides magnetite NPs such as chemical precipitation method (Maity et al. 2010), thermal decomposition of the organic iron precursor in organic solvents (El-Ghandoor et al. 2012), polyol process (Rockenberger et al. 1999), sol–gel method (Cai and Wan 2007), sonochemical synthesis (Dang et al. 2009) and solvothermal synthesis (Zhang et al. 2011). Although most of these methods could produce pure and well-defined NPs, they are relatively expensive and dangerous to the environment (Bhattacharya and Rajinder 2005). Green synthesis methods have many advantages such as the (1) reduction or elimination of hazardous wastes, (2) utilization of sustainable processes, (3) uses of eco-friendly chemicals, solvents or renewable materials (El-Said et al. 2014). Inactivated plant tissue (Padil and Cerník 2013), plant extracts (Shameli et al. 2012), exudates

Editorial responsibility: Binbin Huang

✉ D. M. Fouad  
dinafouad93@hotmail.com

<sup>1</sup> Department of Chemistry, Faculty of Science, Assiut University, Assiut 71516, Egypt

(Lukman et al. 2011) and other parts of living plants (Parsons et al. 2007) were used as environmentally friendly, non-toxic and safe reagents for synthesis of metal NPs (Salam et al. 2012).

Tannin “gallotannic acid or tannic acid” is a mixture of pentadin alloy glucose, pentagalloyl glucose and proanthocyanidins that could be extracted from several plant sources as a colloidal solution in water. Due to its chemical structure (Scheme 1), it could be used as a reducing agent (Cataldo et al. 2013).

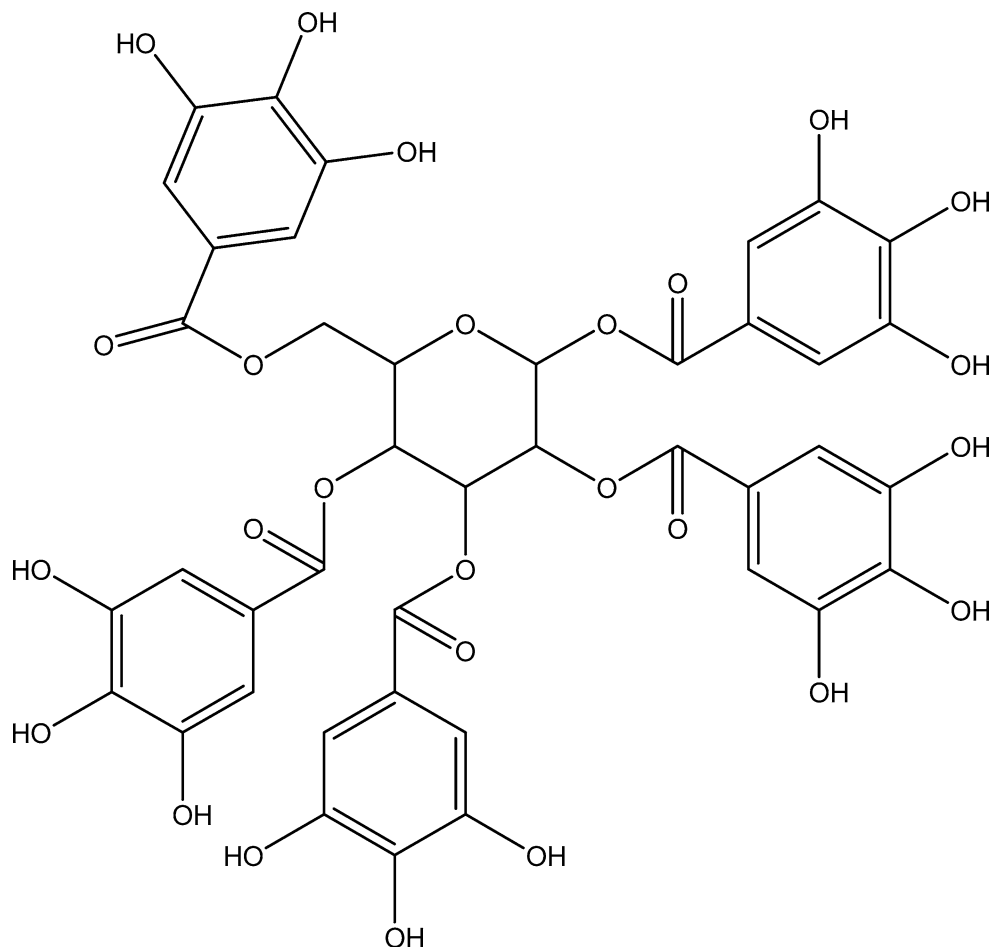
Lindane is one of the organochlorine pesticides, which is considered as an environmental hazard that have an estimated 9.3% dermal absorption rate and is absorbed even more efficiently across abraded skin (Yavuz et al. 2007).

Several methods including catalytic dechlorination (Simagina et al. 2003), photolysis (Wang et al. 2007), hydrothermal decomposition (Prabowo et al. 2007), reductive dechlorination (Chang et al. 2008), bacterial degradation (Fouad and Mohamed 2011) and photodegradation process (Fouad et al. 2015) were applied for the decomposition of different types of pesticides “especially organochlorine pesticides” from water.

Due to the high stability of organochlorine pesticides in for many years after their use (Shukla et al. 2006), thus their removal by different degradation processes showed a low efficiency. And in some instances, decomposition of pesticides results in transformation products that are more toxic, so they represent a greater risk to the environment than the parent molecule (Bavcon et al. 2003). Among the different methods for water treatment, the adsorption method by using solid adsorbents has many advantages over the other methods; these advantages include the simple design, ease of using, low cost and ability for recycling of the adsorbents. Much progress has been made in recent years on adsorption application by using different materials. Developing new adsorbent materials with high efficiency and economic feasibility to remove these pollutants is in demand to improve the water quality.

Mesoporous silica nanoparticles (MSNPs) have received increasing attention in several scientific and technical fields due to their unique features including large surface area, capability for interacting with atoms, ions and molecules on their surfaces and along their porous networks (Akhtar et al. 2015; El-Said et al. 2010).

**Scheme 1** Chemical structure of tannin molecule



Fouad et al. have previously reported on fabrication of silica–gold nanocomposites for removal of methacryfos (methyl (E)-3-dimethoxyphosphinothioxyloxy-2-methylprop-2-enoate) pesticides that show high ability for removal of organophosphorus pesticides up to 90% (Fouad et al. 2017). However, there is a high need for the fabrication of cost-effective materials that have ability to capture the pesticides molecules. Nanomaterials have wide applications in several fields including, chemistry and environment, energy, medicine, agriculture, information and communication, heavy industry (El-Said et al. 2011; Chen et al. 2012; Wang and Chen 2016). The nanomaterials may be unsafe for the biological system, since some of these materials could enter in the body due to the small size and their higher specific surface area and be a toxic at the cellular level (Vishwakarma et al. 2010; Jin et al. 2005). Also, they could easily bind with and transport toxic pollutants, which when inhaled can cause a number of pulmonary diseases in mammals. However, iron oxide nanoparticles ( $\text{Fe}_3\text{O}_4$  NPs) are one of the biocompatible materials that have been widely used for many biotechnology and medical applications such as in magnetic resonance imaging, cell recognition and drug delivery (Laurent et al. 2008; Jain et al. 2005; Modo and Bulte 2005), in addition to some clinical applications including detection of liver tumors, metastatic lymph nodes, inflammatory and degenerative diseases. Therefore, we have selected  $\text{Fe}_3\text{O}_4$  NPs as eco-friendly materials that also enable easy method for extraction from the medium by using external magnetic field.

In the present work, we reported a fast, non-toxic, and green synthesis of magnetite MSNPs/ $\text{Fe}_3\text{O}_4$  nanocomposites by using extractions from green tea as reducing and capping agents. The aim of this work is using MSNPs/ $\text{Fe}_3\text{O}_4$  nanocomposite as a solid adsorbent material for the removal and detection of organochlorine pesticides (lindane). The magnetic feature of the developed MSNPs/ $\text{Fe}_3\text{O}_4$  nanocomposites is an additional advantage for magnetic separation of organochlorine pesticides from wastewater based on applying an external magnetic field as shown in Scheme 2. Our results indicated that we have developed a simple and rapid method to remove lindane from water by using green-synthesized MSNPs/ $\text{Fe}_3\text{O}_4$  nanocomposite with high efficiency.

This work has been started in May 2016, and it was carried out at the laboratories of Faculty of Science, Assiut University.

## Materials and methods

### Materials

Tetraethyl orthosilicate (TEOS,  $\geq 99.9\%$ ) was obtained from Merck; cetyltrimethylammonium bromide (CTAB,  $\geq 98\%$ ) was purchased from Sigma-Aldrich. Ferric chloride and ammonia solution ( $\text{NH}_4\text{OH}$ , 32%) were obtained from Alpha Chemika. Standard pesticide such as lindane was purchased from Riedel-de Haën. All other chemicals and solvents were obtained as an analytical grade and used without any purification. All the solutions were prepared with deionized water (18.2 M $\Omega$  cm), which was purified with a Purite purification system.

### Preparation of MSNPs

MSNPs were prepared by using CTAB surfactant as the structure-directing agent according to the previously reported method (Fouad et al. 2017). In a typical synthesis procedure, 24 mL of deionized water (DIW), 9.6 g of 0.5 M NaOH and 1.0 g of CTAB were added in 100-mL beaker under vigorous stirring at room temperature. 2 mL of TEOS as the silicon source was dropwise added to the mixture and stirred continuously for 8 h. The product material was filtered off, washed three times with DIW and ethanol, and then, dried overnight at 60 °C. The final product was calcined at 550 °C for 5 h to remove all CTAB from the MSNPs.

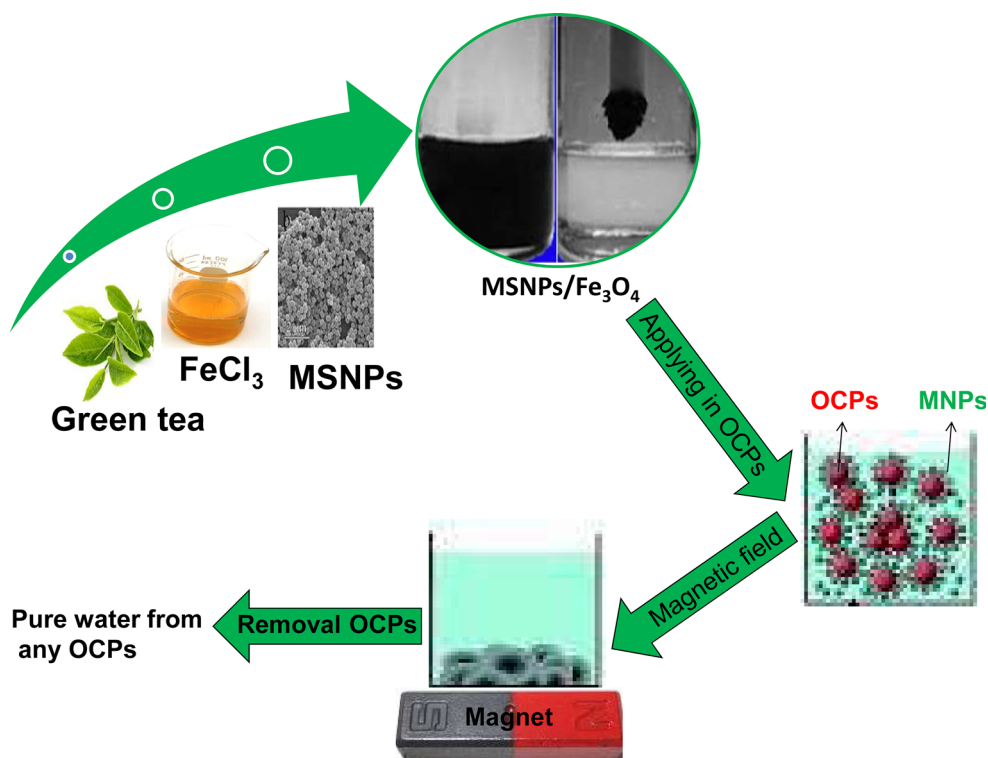
### Preparation of two types of green tea extractions

Two types of extractions were obtained from green tea leaf and used for the synthesis of MSNPs/ $\text{Fe}_3\text{O}_4$  nanocomposite as following:

- (1) The first type of the green tea leaf extraction (total extraction) was obtained by boiling about 5 g of dried green tea in 50 mL of DIW for 60 min, the color of the aqueous solution was changed from watery to yellow and the mixture was allowed to cool to room temperature. The aqueous extract of green tea was separated by filtration with Whatman filter paper and centrifuged at 1000 rpm for 5 min to remove any heavy biomaterials.
- (2) Second type of the green tea leaf extraction (tannin extraction) was prepared by boiling about 5 g of dried green tea in 50 mL of ethanol for 60 min. The mixture was allowed to cool to room temperature and to evaporate ethanol under vacuum evaporation to obtain the tannin.



**Scheme 2** Graphical scheme for removal of lindane



### Green synthesis of $\text{MSNPs/Fe}_3\text{O}_4$ nanocomposites

Magnetite  $\text{MSNPs/Fe}_3\text{O}_4$  nanocomposite was synthesized based on using tea extraction as follows:

Typically, 0.4 g of the prepared MSNPs was dispersed in 50 mL of DIW, and then, 1.11 gm of  $\text{FeCl}_3 \cdot 6\text{H}_2\text{O}$  was added, and the solution heated at 80 °C under mild stirring for 10 min. Then, 50 mL of tea extractions was added, and immediately the yellowish color of the ferric chloride solution changed into reddish brown color and its pH was strong acidic (about 1). After 5 min, hot ammonia aqueous solution was added to the mixture until it became alkaline (about pH = 8).  $\text{NH}_4\text{OH}$  was added with rate of 1 mL/min for allowing the precipitation of magnetite uniformly under mild stirring for about 60 min at 100 °C. The mixture was allowed to cool down to room temperature. And the  $\text{MSNPs/Fe}_3\text{O}_4$  nanocomposite was purified by washing three times by using DIW and ethanol. Finally, the  $\text{MSNPs/Fe}_3\text{O}_4$  nanocomposites were dried overnight at 80 °C and calcined at different annealing temperatures for 5 h.

### Measurements

The chemical, crystal structure and morphologies of MSNPs and  $\text{MSNPs/Fe}_3\text{O}_4$  nanocomposites were characterized by HRTEM analysis by using a JEOL-2000 instrument operated at high voltage 120 kV. X-ray diffraction (XRD) analysis of test samples was performed

with a Philips (The Netherlands) diffractometer (Model PW 2103,  $\lambda = 1.5418 \text{ \AA}$ , 35 kV and 20 mA) with a source of  $\text{CuK}\alpha$  radiation (Ni-filtered). The diffraction patterns were recorded in the range of the diffraction angle  $2\theta$  from 10° to 90° with a step of 0.06°. Fourier transform infrared (FTIR) spectra of MSNPs and  $\text{MSNPs/Fe}_3\text{O}_4$  nanocomposite were measured by using a Nicolet™ iS™10 FTIR spectrometer in the wave number range 400–3800  $\text{cm}^{-1}$ . The samples have been admixed with KBr under vacuum and at pressure of 1.88 tons/ $\text{cm}^2$ . Thermogravimetric analysis (TGA) was conducted by using Shimadzu thermogravimetric analyzer model (TGA-60H) in the temperature range of 0–750 °C, with a heating rate of 10 °C/min under air atmosphere. Nitrogen adsorption was recorded for mesoporous silica using a model NOVA 3200 automated gas sorption system (quanta chrome, USA). Magnetic properties of the samples were measured using a vibration sample magnetometer (VSM; susceptibility meter 4700). UV-Vis spectroscopy double beam PC scanning spectrophotometer UV Evolution 300 from Labomed a computer data system is UV Win 5 software v 5.0.5 used for measuring wavelength and absorbance. Spectrophotometer range from 200 to 900 nm using 1-cm matched Stoppard quartz cells was used for monitoring the rate of pesticides removal. High-performance liquid chromatography (HPLC) for the tested samples was promptly analyzed using Agilent 1100 high-performance liquid chromatography system fitted with a diode array detector



and an autosampler. Gas chromatograph (GC) using Agilent 6890 equipped with a Ni<sup>63</sup> electron capture detector. Raman spectra were recorded with a Bruker Senterra Raman microscope (Bruker Optics Inc., Germany) with 785 nm excitation, 1200 rulings mm<sup>-1</sup> holographic grating and a charge-coupled device (CCD) detector. The acquisition time was 3 s with power of 50 mW.

## Results and discussion

### Chemical and structural features of MSNPs and MSNPs/Fe<sub>3</sub>O<sub>4</sub> nanocomposite

In the present work, MSNPs have been synthesized using TEOS as source of silicon in the presence of CTAB as a cationic surfactant under basic conditions. The chemical, morphological and cryptographical features of the prepared MSNPs and MSNPs/Fe<sub>3</sub>O<sub>4</sub> nanocomposite were investigated, also the optimum conditions for the preparation of MSNPs/Fe<sub>3</sub>O<sub>4</sub> nanocomposite, were investigated by using the SEM, HRTEM, FT-IR, EDX, XRD, nitrogen adsorption and Raman spectroscopic analyses.

#### *Effect of concentration of green tea extracts on the crystallography and structure of Fe<sub>3</sub>O<sub>4</sub> NPs*

In order to optimize the green synthesis of Fe<sub>3</sub>O<sub>4</sub>, we have used different concentrations of the tea extractions to investigate the effect of the amount of tea on the chemical structure of iron oxide NPs by using XRD. Figure 1a–c shows the XRD patterns of the as-prepared iron oxide NP samples by using different amounts of green tea (1, 5 and 8 gm) to reduce 1.11 gm of FeCl<sub>3</sub>·6H<sub>2</sub>O; these results demonstrated that using the extraction from 1 gm of green tea results in obtained Fe<sub>2</sub>O<sub>3</sub> NPs as shown in Fig. 1a. By increasing the amount of green tea until 5 gm, Fe<sub>3</sub>O<sub>4</sub> NPs was obtained (Fig. 1b). Furthermore, by increasing the amount of extracted tea over 5 gm results in decreasing the intensity of the XRD peaks that related to the adsorption of green tea extraction onto the surface of Fe<sub>3</sub>O<sub>4</sub> NPs (Fig. 1c). Thus, we have selected the usage of the extraction from 5 gm of green tea as optimum amount of tea under these conditions for the further experiments.

#### *Structure analysis and phase change of Fe<sub>3</sub>O<sub>4</sub> NPs*

To obtain Fe<sub>3</sub>O<sub>4</sub> NPs in pure form, we have studied the effect of annealing temperature on the chemical structures as well as the crystallography of the Fe<sub>3</sub>O<sub>4</sub> NPs. Figure 2a–d shows the XRD patterns of the as-prepared iron oxide NPs and calcined samples at different annealing temperatures (200, 400 and 600 °C). These results reveal several

prominent peaks at  $2\theta$  values including 32.82°, 35.40°, 44.17°, 49.35°, 53.71° and 63.87°, which well matched with the planes (220), (311), (222), (400), (422) and (511), respectively; these results indicated the formation of Fe<sub>3</sub>O<sub>4</sub> monoclinic structure [reference: POWD:01-089-0951]. In addition, the intensity of all XRD peaks was increased by increasing the annealing temperature that indicates the decomposition of the all organic materials (tea's extraction) and increase in the crystallinity of Fe<sub>3</sub>O<sub>4</sub> NPs.

#### *Uses of tannin extraction for the fabrication of Fe<sub>3</sub>O<sub>4</sub> NPs and MSNPs/Fe<sub>3</sub>O<sub>4</sub> nanocomposite*

Furthermore, we have used tannin extracted instead of total extraction from green tea for synthesis of Fe<sub>3</sub>O<sub>4</sub> NPs. Figure 3a shows the XRD pattern of the as-prepared iron oxide NPs that have been prepared by using tannin, which indicated the formation of Fe<sub>3</sub>O<sub>4</sub> NPs. Thus, tannin is the active ingredient compound in green tea that is responsible for the formation of Fe<sub>3</sub>O<sub>4</sub> NPs. Finally, we have applied the optimum conditions for fabrication of MSNPs/Fe<sub>3</sub>O<sub>4</sub> based on deposition of Fe<sub>3</sub>O<sub>4</sub> onto MSNPs in the presence of tannin as a reducing agent. Figure 3b represents the XRD pattern of MSNPs/Fe<sub>3</sub>O<sub>4</sub> nanocomposite, which demonstrated the appearance of a new peak at  $2\theta$  equal 23° accredited to (100) that indicates the successful formation of MSNPs/Fe<sub>3</sub>O<sub>4</sub> nanocomposite.

#### *Chemical and structural features of MSNPs/Fe<sub>3</sub>O<sub>4</sub> nanocomposite*

The surface morphologies of MSNPs and MSNPs/Fe<sub>3</sub>O<sub>4</sub> nanocomposite have been studied by using SEM. Figure 4a, b represents the SEM images of MSNPs and MSNPs/Fe<sub>3</sub>O<sub>4</sub> nanocomposite, respectively, which indicated the formation of tiny MSNPs; aggregation of the particles and small grains are present at the surface. In addition, Fig. 4c, d shows the HRTEM images of MSNPs and MSNPs/Fe<sub>3</sub>O<sub>4</sub> nanocomposite, respectively, which indicate the formation of a quasi-spherical in shape MSNPs/Fe<sub>3</sub>O<sub>4</sub> with polydispersed size distribution. The aggregation of small nanocomposite is a result of magnetic features effects during the preparation of MSNPs/Fe<sub>3</sub>O<sub>4</sub> nanocomposite for HRTEM analysis. TGA of the as-prepared MSNPs/Fe<sub>3</sub>O<sub>4</sub> nanocomposite is shown in Fig. 5 that represented the weight loss versus temperature until 750 °C in air, which demonstrated the presence of three weight loss stages. The first stage showed weight loss of about 7.931% in the sample at around 195 °C that likely is due to the elimination of the water molecules absorbed by MSNPs/Fe<sub>3</sub>O<sub>4</sub> nanocomposite. The second stage demonstrated weight loss of about 6.265% in the sample at around

**Fig. 1** XRD pattern of the as-prepared  $\text{Fe}_3\text{O}_4$  NPs using total extraction from **a** 1 g of green tea, **b** 5 g of green tea and **c** 8 g of green tea

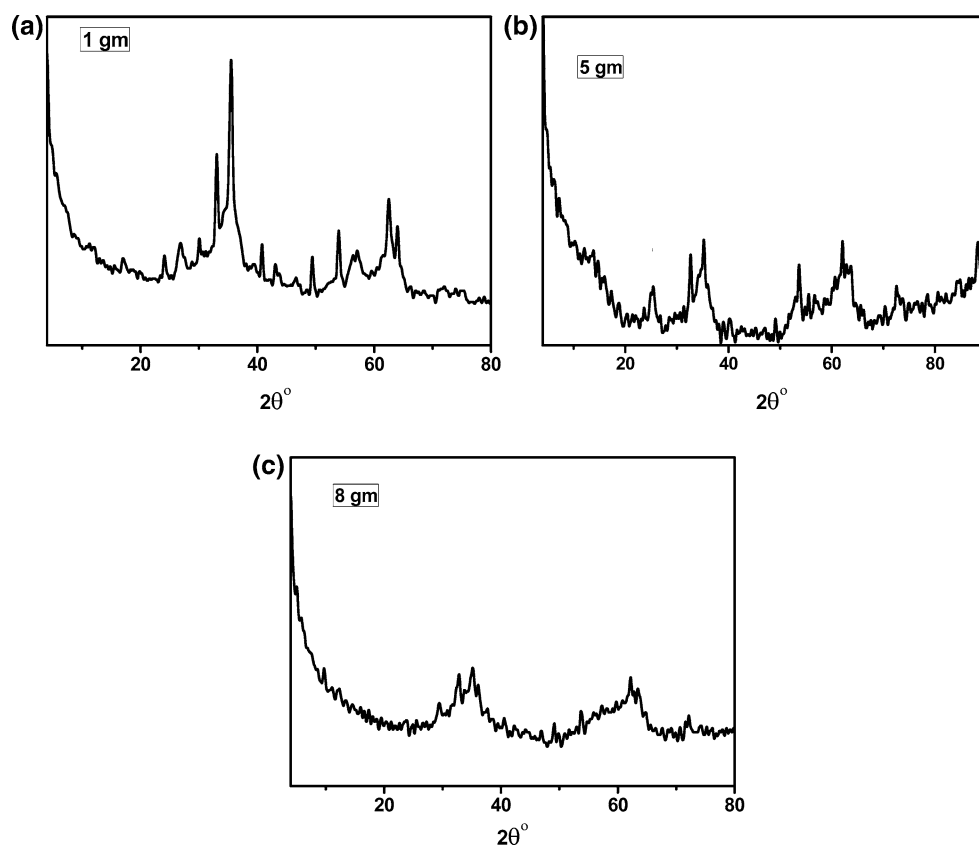


**Fig. 2** XRD pattern of the **a** as-prepared  $\text{Fe}_3\text{O}_4$  NPs, **b**  $\text{Fe}_3\text{O}_4$  NPs annealed at  $200^\circ\text{C}$ , **c**  $\text{Fe}_3\text{O}_4$  NPs annealed at  $400^\circ\text{C}$  and **d**  $\text{Fe}_3\text{O}_4$  NPs annealed at  $600^\circ\text{C}$

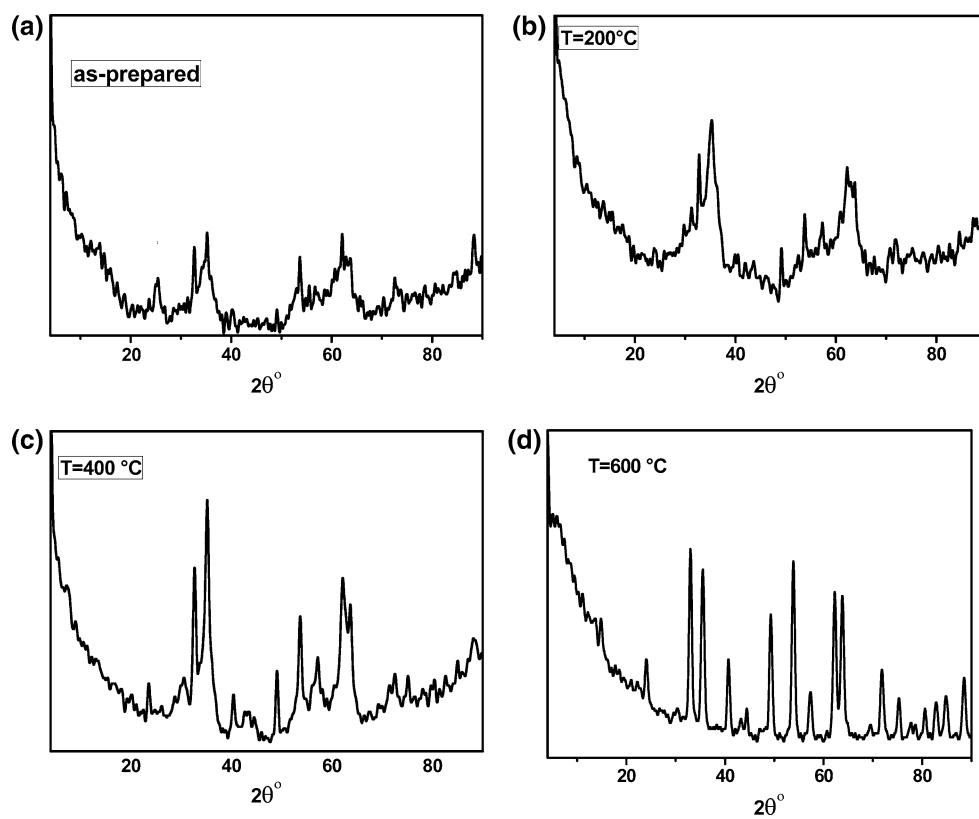


**Fig. 3** XRD pattern of **a** as-prepared  $\text{Fe}_3\text{O}_4$  NPs by using tannin and **b** MSNPs/ $\text{Fe}_3\text{O}_4$  nanocomposite

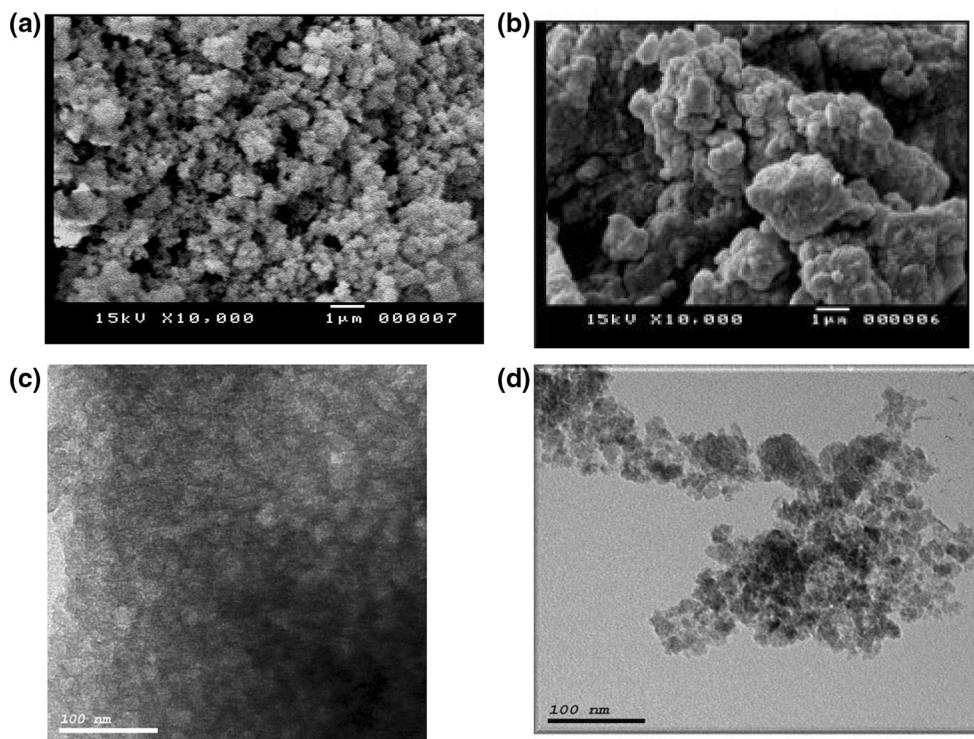
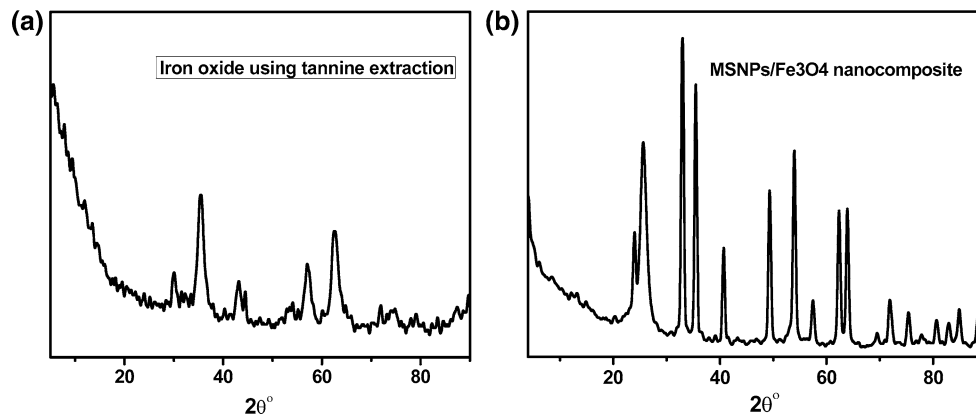


**Fig. 4** **a** SEM of MSNPs, **b** SEM of MSNPs/ $\text{Fe}_3\text{O}_4$  nanocomposite, **c** HRTEM of  $\text{Fe}_3\text{O}_4$  and **d** HRTEM of MSNPs/ $\text{Fe}_3\text{O}_4$  nanocomposite

410 °C that could be caused by the decomposition of the tea extractions that absorbed on the nanocomposite surface. The third stage showed the presence of little weight loss of about 2.499% at about 600 °C that could be related to the decomposition of the residual organic materials of the tea extracts, and then, the sample weight was almost constant, which indicates the thermal stability of the sample. Figure 6a shows the FT-IR spectra of MSNPs and MSNPs/ $\text{Fe}_3\text{O}_4$  nanocomposite, indicating that the  $\text{Fe}_3\text{O}_4$  molecules were deposited onto silica NPs. FT-IR spectrum of MSNPs shows a broad peak at 1077  $\text{cm}^{-1}$ , which could be assigned to Si—O—Si bond of silica, and the peak at 960  $\text{cm}^{-1}$  can be attributed to Si—OH bond and broad peak at 3400  $\text{cm}^{-1}$  that corresponding to O—H bond. FTIR spectrum of

MSNPs/ $\text{Fe}_3\text{O}_4$  nanocomposite (Fig. 6a) demonstrated that functionalized silica particles with iron molecules result in reducing the intensity of Si—O—Si and Si—OH peaks significantly, also the deposition of  $\text{Fe}_3\text{O}_4$  molecules was characterized by two strong absorption peaks at around 560 and 440  $\text{cm}^{-1}$ , which correspond to the Fe—O stretching vibration band of  $\text{Fe}_3\text{O}_4$  (Wu et al. 2004). Raman spectroscopy was also used to confirm the deposition of  $\text{Fe}_3\text{O}_4$  into MSNPs; Fig. 6b shows the Raman spectrum of MSNPs, which revealed a peak at 1363  $\text{cm}^{-1}$  corresponding to mesoporous silica ( $\text{SiO}_2$ ), while Raman spectrum of MSNPs/ $\text{Fe}_3\text{O}_4$  nanocomposite (Fig. 6b) demonstrated the appearance of two new wide peaks at 730 and 1438  $\text{cm}^{-1}$  corresponding to  $\text{Fe}_3\text{O}_4$  phases, which

## Thermal Analysis Result

Detector: DTG-60H  
 Sample Name: Fe  
 Sample Weight: 15.546[mg]  
 Cell: Platinum  
 Atmosphere: Nitrogen  
 Flow Rate: 40[mL/min]

Assiut University  
 Central Lab.  
 Thermal Analysis Unit

[Temp Program]  
 Temp Rate Hold Temp Hold Time  
 [C/min] [ C ] [ min ]  
 10.00 750.0 0

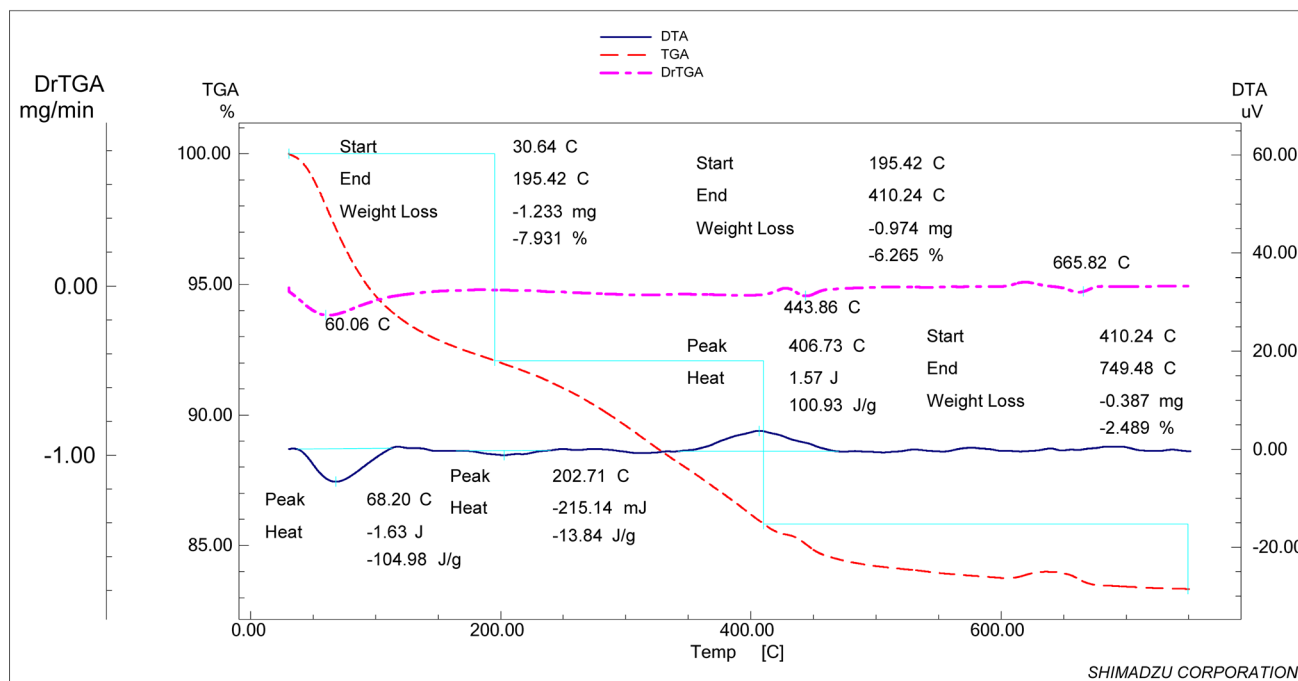


Fig. 5 TGA of MSNPs/Fe<sub>3</sub>O<sub>4</sub> nanocomposites

indicated the formation of MSNPs/Fe<sub>3</sub>O<sub>4</sub> nanocomposites. Furthermore, EDX spectral analysis of MSNPs/Fe<sub>3</sub>O<sub>4</sub> nanocomposites reveals the presence of carbon, silicon, oxygen and iron in synthesized nanocomposite as shown in Fig. 6c. The appearance of peak of carbon in EDX spectra is due to the presence of organic molecules (tea extracts).

#### Magnetic measurements

The magnetic behavior of the prepared MSNPs/Fe<sub>3</sub>O<sub>4</sub> nanocomposite was performed by using VSM at room temperature. Figure 6d shows the hysteresis loop obtained from the magnetization (*M*) versus field (*H*) data for MSNPs/Fe<sub>3</sub>O<sub>4</sub>. The magnetic hysteresis loop (*M*–*H* curve) of MSNPs/Fe<sub>3</sub>O<sub>4</sub> nanocomposite demonstrated a typical behavior of ferromagnetic materials at room temperature. The value of their saturation magnetization (*M<sub>s</sub>*) was 40 emu/g. The excellent magnetic feature was necessary for magnetic separation of organochlorine pesticides from wastewater by applying an external magnetic field on MSNPs/Fe<sub>3</sub>O<sub>4</sub> nanocomposite (Lu et al. 2004). The mag-

netic susceptibility of the materials was demonstrated in a simple laboratory setup with a handheld magnet. MSNPs/Fe<sub>3</sub>O<sub>4</sub> nanocomposite could be completely separated from the aqueous solution within 5 min.

#### Nitrogen sorption isotherm

The morphology and surface features of the prepared MSNPs and MSNPs/Fe<sub>3</sub>O<sub>4</sub> nanocomposite were characterized using the nitrogen sorption isotherm (Nunes et al. 2006). Analysis of the nitrogen adsorption/desorption branches of MSNPs showed a BET surface area of 818 m<sup>2</sup>/g and a total pore volume of 0.64 cm<sup>3</sup>/g. The pore size, calculated from the desorption isotherm using the BJH theory, was found to be 33 Å in diameter with a uniform distribution. MSNPs/Fe<sub>3</sub>O<sub>4</sub> nanocomposite has been fabricated based on deposition of Fe<sub>3</sub>O<sub>4</sub> onto MSNPs by using total green tea extraction and tannin extraction. Our results demonstrated that loading of Fe<sub>3</sub>O<sub>4</sub> particles onto the surface of MSNPs results in decrease in the BET surface area to become 93.12 m<sup>2</sup>/g as shown in Table 1.





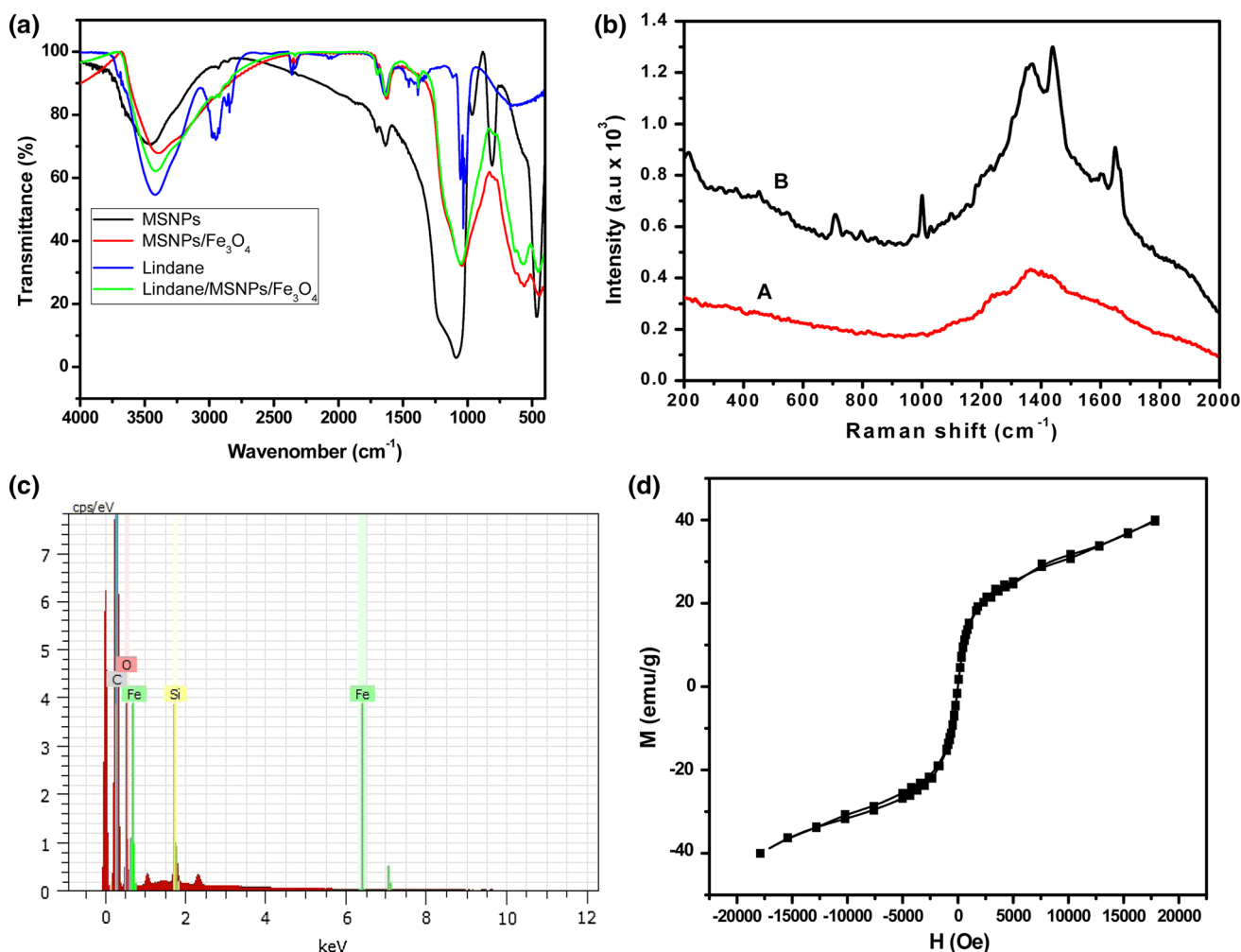


**Fig. 6** a FTIR spectra of MSNPs, MSNPs/Fe<sub>3</sub>O<sub>4</sub> nanocomposite, pure lindane and lindane adsorbed onto MSNPs/Fe<sub>3</sub>O<sub>4</sub> nanocomposite, b Raman spectra of MPSNPs and MSNPs/Fe<sub>3</sub>O<sub>4</sub> nanocomposite,

c EDX image of MSNPs/Fe<sub>3</sub>O<sub>4</sub> nanocomposite and d Magnetization curve of MSNPs/Fe<sub>3</sub>O<sub>4</sub> nanocomposite at room temperature

**Table 1** Surface area and pore volume of the synthesized MSNPs and MSNPs/Fe<sub>3</sub>O<sub>4</sub> nanocomposites

Sample	<i>S</i> <sub>BET</sub> (m <sup>2</sup> /g)	<i>V</i> <sub>p</sub> (cm <sup>3</sup> /g)	<i>R</i> (Å)
MSNPs	818	0.7	33
MSNPs/Fe <sub>3</sub> O <sub>4</sub>	93	0.31	58

**Detection of lindane using the MSNPs/Fe<sub>3</sub>O<sub>4</sub> nanocomposite**

The high stability of the organochlorine pesticides and their long resistance time in the environment is an environmental challenge; therefore development of simple, easy of use, cost-effective with high capability for recycling adsorption process by using solid adsorbents is urgently needed. The absorption of lindane by using MSNPs/Fe<sub>3</sub>O<sub>4</sub>

nanocomposite as solid adsorbent was confirmed by FT-IR technique. As shown in Fig. 6a, pure lindane showed its characteristic peaks, especially the functionality of C–Cl was observed at 1385 cm<sup>-1</sup>. Upon the binding of MSNPs/Fe<sub>3</sub>O<sub>4</sub> nanocomposite, the increase and shift of FTIR peaks were observed, which confirmed the adsorption of lindane into MSNPs/Fe<sub>3</sub>O<sub>4</sub> nanocomposite.

**Removal of lindane using the MSNPs/Fe<sub>3</sub>O<sub>4</sub> nanocomposite**

Purification of water from the pesticides traces represents an environmental challenge due to their high stability and long resistance time in the environment. Here, we have applied MSNPs, Fe<sub>3</sub>O<sub>4</sub> and MSNPs/Fe<sub>3</sub>O<sub>4</sub> nanocomposite as a solid sorbent for removal of lindane at low concentration. In order to optimize the conditions of the removal process and the removal efficiency of MSNPs/Fe<sub>3</sub>O<sub>4</sub> nanocomposite, we

have investigated the effects of temperature and pH of the medium. Figure 7a shows the UV-Vis spectra of lindane before and after being treated with MSNPs/Fe<sub>3</sub>O<sub>4</sub> nanocomposite for different treatment periods up to 7 h, which illustrated that the UV-Vis spectrum of standard solution of lindane showed an absorbance peak at wavelength of about 273 nm and the intensity of this absorption peak was decreased with the increase in the contact time. Figure 7b shows the time profile of lindane removal with MSNPs/Fe<sub>3</sub>O<sub>4</sub> nanocomposite, which indicated that the uptake percentage of lindane was increased with the increase in the contact time until reaching the saturation phase after 5 h. Also, it confirmed that the lindane adsorption is a rapid process with almost 60% lindane being removed within approximately 5 h, which indicates the high affinity between the lindane pesticide and the MSNPs/Fe<sub>3</sub>O<sub>4</sub> nanocomposite. Furthermore, we have studied the behavior of lindane pesticide in solutions of different pH values within the range from 3 to 12. Figure 7c shows the UV-Vis spectra of lindane

in different pH solutions, which showed an absorption peak for lindane in neutral solution centered at about 270 nm, and this peak was shifted to longer wavelengths with the increase in the pH of alkaline solution (pH at 9 or 12) to 286 nm. The shifting of the absorption peak of lindane in alkaline medium dechlorination of lindane indicates that lindane pesticide is unstable in alkaline medium. Thus, we have performed all the next experiments in the neutral medium. Figure 8a shows the absorbance spectra of different concentrations of lindane within range from 1 to 40 ppm, which demonstrated that the intensity of the absorbance peak at wavelength of about 273 nm was increased as the concentration of lindane increased. Figure 8b shows the UV-Vis spectra of 10 ml of lindane pesticide solution (40 ppm) after treatment with a wide range of concentrations of MSNPs; lindane solution showed an absorbance peak at 273 nm, which demonstrated that the intensity of this peak was slightly decreased with the increase in the amount of the solid adsorbent and reached the saturation at 40 mg of MSNPs after stirring for 6 h at room

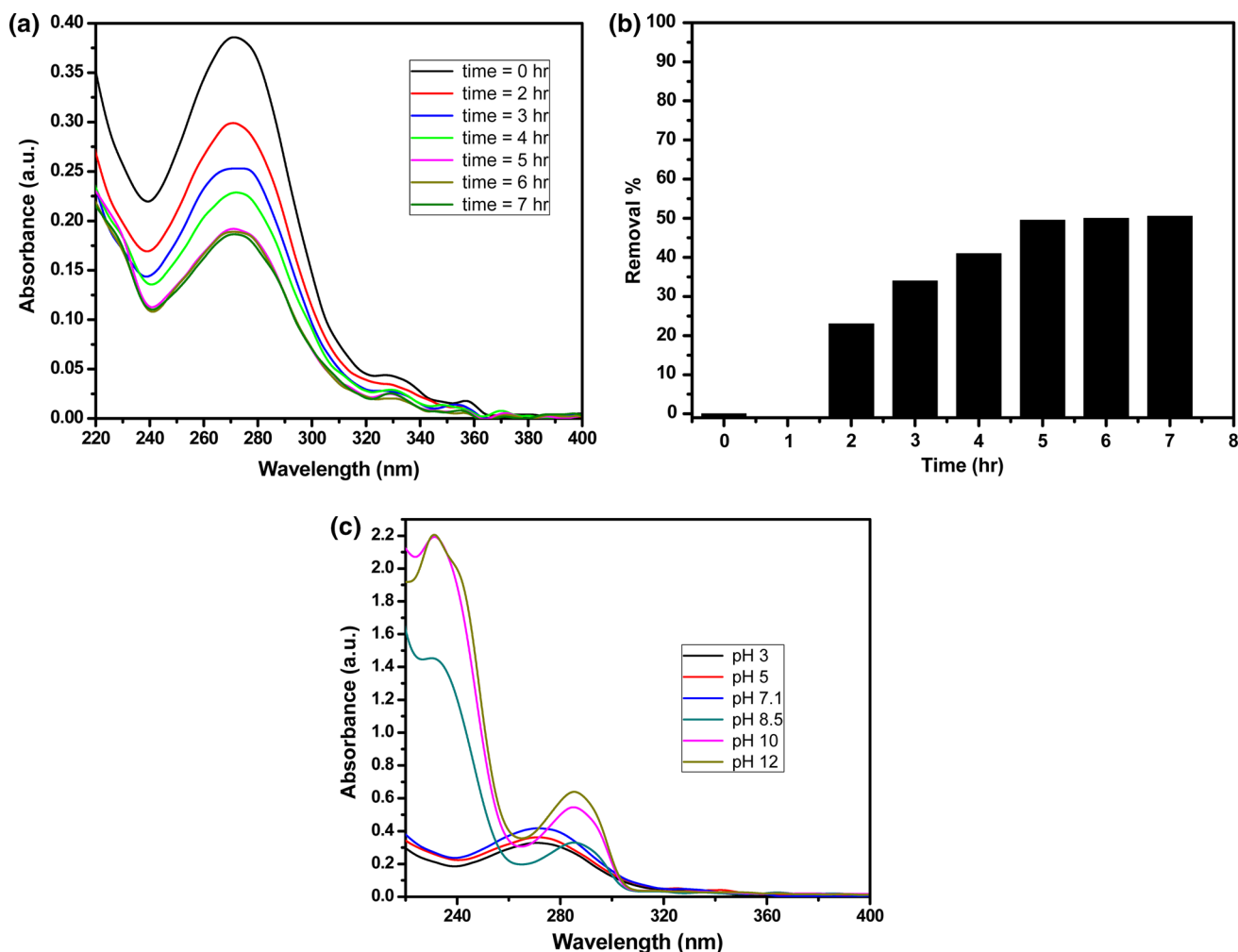


**Fig. 7** a UV spectra of 40 ppm of lindane solution after being treated with 70 mg of Fe<sub>3</sub>O<sub>4</sub>/MSNPs nanocomposite for different treatment time up to 7 h, b influence of the treatment time on the removal percentage, c UV spectra of lindane solution of different pH values from 3 to 12



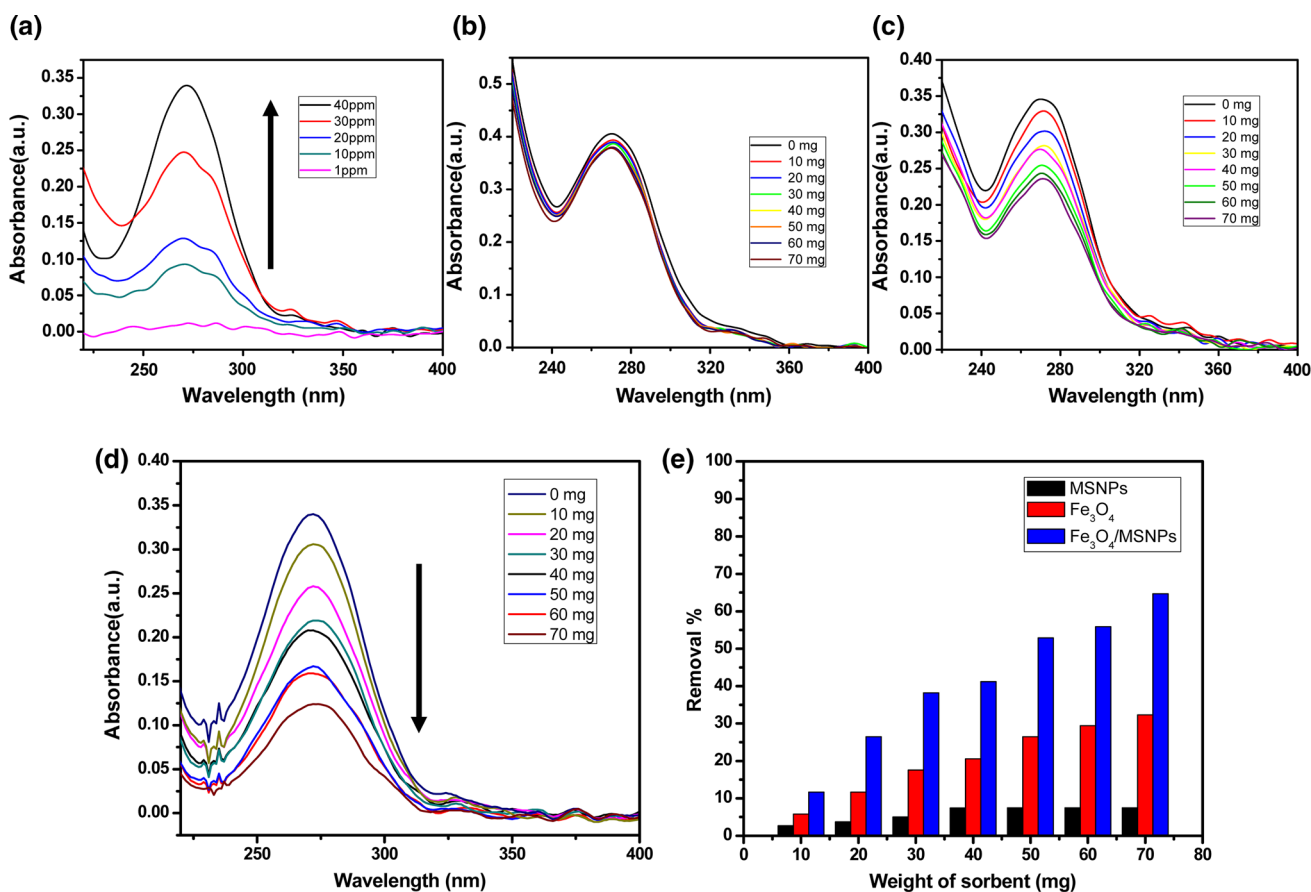


**Fig. 8** **a** UV spectra of different concentrations of lindane solution over range from 1 to 40 ppm, **b** UV spectra of removal lindane by using different amounts of MSNPs, **c** UV spectra of removal lindane by using different amounts of Fe<sub>3</sub>O<sub>4</sub>, **d** UV spectra of removal lindane

by using different amounts of Fe<sub>3</sub>O<sub>4</sub>/MSNPs nanocomposite and **e** influence of amount three different solid adsorbents on removal of lindane

temperature. This weak removal efficiency of MSNPs is due to the difficulty binding between silica surface and the lindane pesticides. Then, we have used the same doses from Fe<sub>3</sub>O<sub>4</sub> NPs for treating the lindane solution as shown in Fig. 8c, which indicated that the intensity of the absorption peak of lindane was decreased, and this decreasing was higher than that observed by using the same amount of MSNPs. Finally, we have used the same doses from Fe<sub>3</sub>O<sub>4</sub>/MSNPs nanocomposite for treating the lindane solution that showed the strongest decrease in the absorption in comparison with MSNPs or Fe<sub>3</sub>O<sub>4</sub> at the same dose (Fig. 8d). Figure 8e shows the relationship between the removal efficiency and the amount of adsorbent, which indicated the removal percentage of lindane by using the same range of amounts of MSNPs, Fe<sub>3</sub>O<sub>4</sub> or Fe<sub>3</sub>O<sub>4</sub>/MSNPs nanocomposite, which demonstrated that for the treatment of the lindane solution with MSNPs, the maximum removal percentage reached up to 7.5% by using 40 mg of the solid adsorbent; moreover, there is no further effect by increasing the amount of adsorbent over 40 mg. But in case of the usage of Fe<sub>3</sub>O<sub>4</sub>

for the treatment, the maximum removal percentage reached up to 30% by using 60 mg. On the other hand, usage of Fe<sub>3</sub>O<sub>4</sub>/MSNPs nanocomposite as solid adsorbent for the treatment of lindane solution shows the highest removal percentage that reached 65% by using 70 mg of the nanocomposite, due to the large surface area and the high capability of Fe<sub>3</sub>O<sub>4</sub>. So, functionalization of mesoporous silica with Fe<sub>3</sub>O<sub>4</sub> is an important issue for the removal of lindane solution, since the mechanism of removal depends on the interaction between the chlorine atoms of lindane and the Fe<sub>3</sub>O<sub>4</sub> NPs. In addition, the excellent magnetic feature was necessary for magnetic separation of lindane pesticides from wastewater by applying an external magnetic field on MSNPs/Fe<sub>3</sub>O<sub>4</sub> nanocomposite to release by using external magnetic field. Furthermore, HPLC technique was used to confirm removal of lindane by using MSNPs/Fe<sub>3</sub>O<sub>4</sub> nanocomposite. HPLC technique showed that lindane has one sharp peak at retention time of 3.2 min; the decrease in the area of this band intensity and the area under the peak reflects the removal of the lindane. These results shown in

Fig. 9a, b demonstrated that by the increase in the addition of MSNPs/Fe<sub>3</sub>O<sub>4</sub> nanocomposite amount to lindane solution, a marked decrease in the peak area and the integration area percentage was observed. From Fig. 9c, it was found that using of 60 mg of MSNPs/Fe<sub>3</sub>O<sub>4</sub> nanocomposite as solid adsorbent results in decreasing the absorbance unit (mAU) from 49 to 14. The effect of sorbent concentrations within range from 0.02 to 0.06 gm on the remove capacity of lindane was investigated by using MSNPs/Fe<sub>3</sub>O<sub>4</sub> nanocomposite. Our results indicated that the amount of adsorbent is an important parameter which affects the ability of a sorbent for a sorbet. Finally, to verify the UV-Vis data for the removal of lindane by using MSNPs/Fe<sub>3</sub>O<sub>4</sub> nanocomposite, we have used GC technique to monitor the lindane removal by using 8 different concentrations of MSNPs/Fe<sub>3</sub>O<sub>4</sub> nanocomposite over a wide range from 10 to 130 mg. Figure 10 shows the GC chromatograms of lindane solution before and after the treatment with different doses of MSNPs/Fe<sub>3</sub>O<sub>4</sub> nanocomposite (10, 30, 50, 70, 90, 110 and

130 mg), which demonstrated that the GC chromatogram of lindane standard solution has one sharp peak at retention time of 2.5 min (Fig. 10a); the band intensity and the area under the peak of lindane solution were decreased as the amount of the solid adsorbent (MSNPs/Fe<sub>3</sub>O<sub>4</sub> nanocomposite) increased (Fig. 10b–h), which reflects the removal of the lindane. Then, we calculated the mole percent of lindane based on the areas under the curves by using Eq. 1, and these data are listed in Table 2, which illustrates that the removal of lindane was increased by increasing the amount of the solid sorbent within range from 10 to 130 mg, and it reached its maximum removal efficiency at 110 mg of MSNPs/Fe<sub>3</sub>O<sub>4</sub> nanocomposite, which is in good agreement with the UV-Vis results. From Eq. (1), GC data indicated that the removal efficiency of the developed solid adsorbent against lindane pesticide was about 99% at 90 mg of MSNPs/Fe<sub>3</sub>O<sub>4</sub> nanocomposite.

$$\text{Mole \% lindane} = (\text{area of Peak}/\text{total area}) \times 100 \quad (1)$$

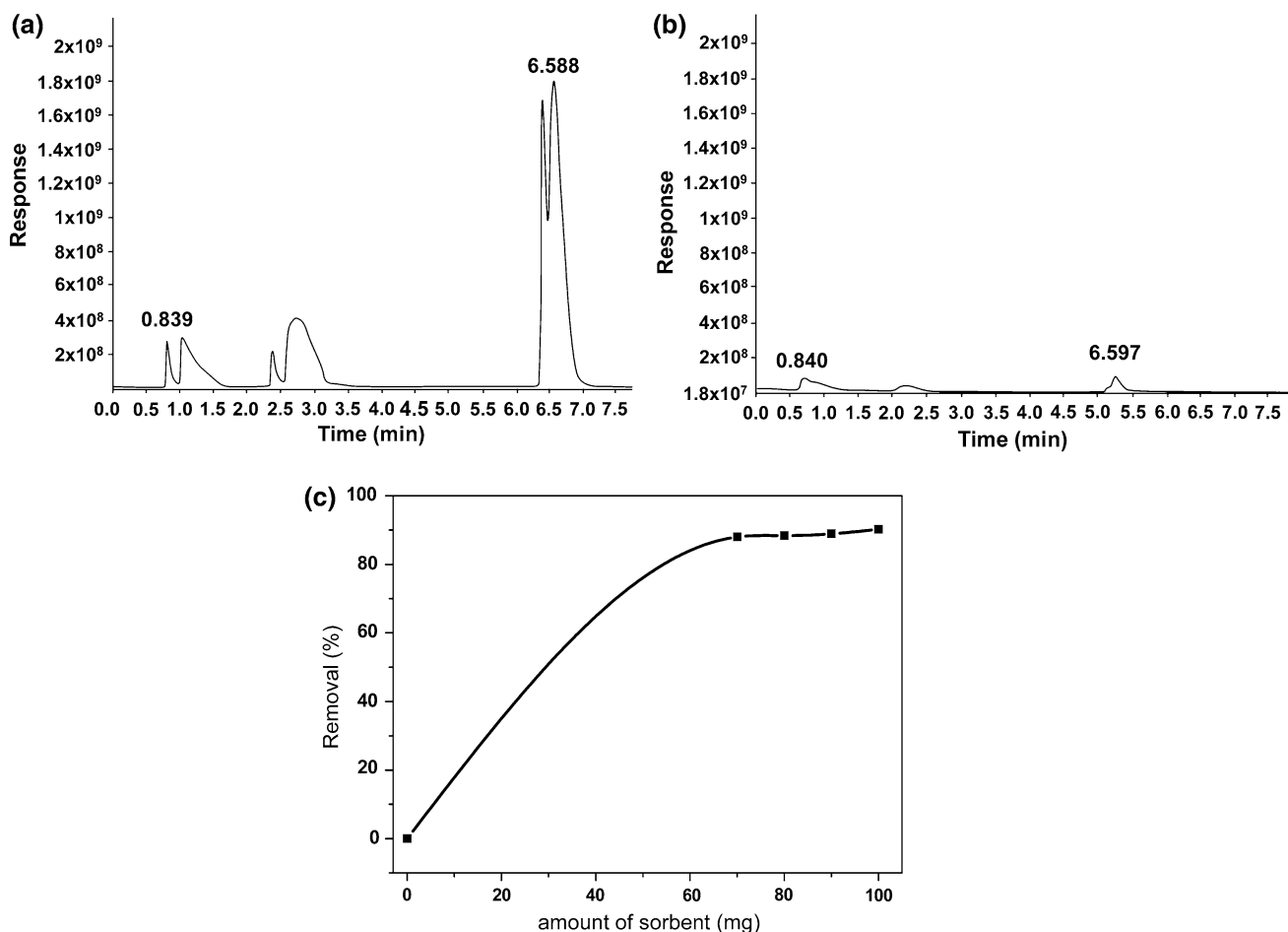


**Fig. 9** a HPLC chromatogram of lindane solution, b HPLC chromatogram of lindane solution after treatment with MSNPs/Fe<sub>3</sub>O<sub>4</sub> nanocomposite and c influence of amount sorbent on removal uptake of lindane



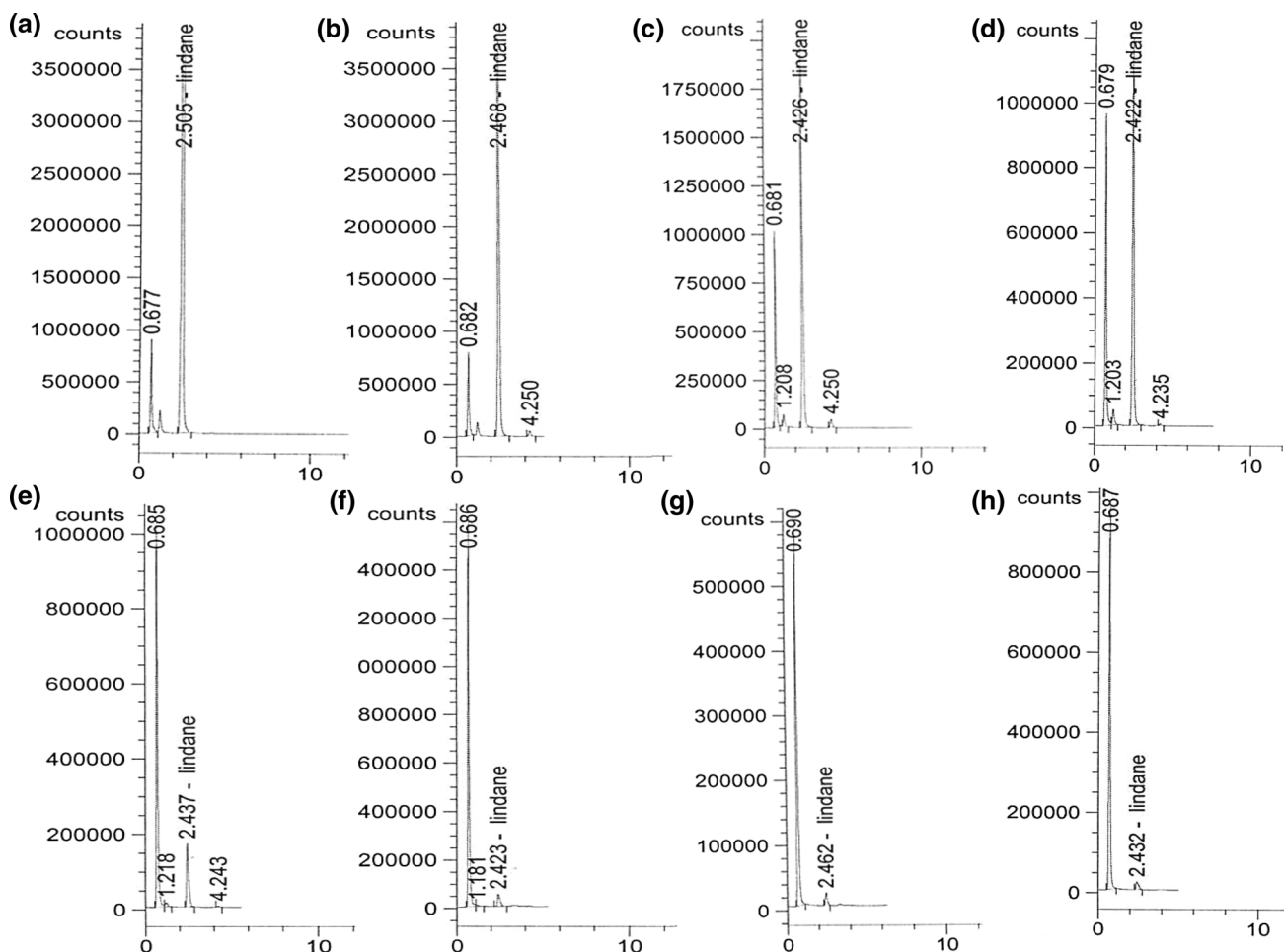


**Fig. 10** GC chromatograms for lindane solution before and after treatment with different doses **a** 0 ppm, **b** 10 ppm, **c** 30 ppm, **d** 50 ppm, **e** 70 ppm, **f** 90 ppm, **g** 110 ppm and **h** 130 ppm of MSNPs/Fe<sub>3</sub>O<sub>4</sub> nanocomposite

**Table 2** Influence of amount of MSNPs/Fe<sub>3</sub>O<sub>4</sub> nanocomposites on the removal uptake based on GC technique

Weight of sorbent (mg)	Mole % of lindane (%)
0	100
10	73.8
30	32.4
50	20.7
70	3.5
90	1.2
110	0.5
130	0.4

**Conclusion**

Here, we have reported a rapid, single step and completely green synthetic method for Fe<sub>3</sub>O<sub>4</sub> particles. The MSNPs/Fe<sub>3</sub>O<sub>4</sub> nanocomposite has been characterized by SEM,

XRD, EDX, FTIR and HRTEM. Particle size analysis of MSNPs/Fe<sub>3</sub>O<sub>4</sub> nanocomposite was 30 nm. MSNPs/Fe<sub>3</sub>O<sub>4</sub> nanocomposite was used in the treatment of water from lindane pesticide as a model of OCP. Removal percentage of this type of pesticides exceeds 99% by using 90 mg of MSNPs/Fe<sub>3</sub>O<sub>4</sub> nanocomposite. This nanocomposite possesses high capability for lindane capture, which could explore a new biocompatible and eco-friendly strategy for pesticide removal, and appears to be the new promising material in water treatment application.

**Acknowledgements** This work was supported by Assiut University.

**References**

Akhtar N, El-Safty SA, Khairy M, El-Said WA (2015) Fabrication of a highly selective nonenzymatic amperometric sensor for hydrogen peroxide based on nickel foam/cytochrome c modified electrode. *Sens Actuators B Chem* 207:158–166  
 Bavcon M, Trebse P, Zupancic-Kralj L (2003) Investigations of the determination and transformations of diazinon and malathion

- under environmental conditions using gas chromatography coupled with a flame ionisation detector. *Chemosphere* 50:595–601
- Bhattacharya D, Rajinder G (2005) Nanotechnology and potential of microorganisms. *Crit Rev Biotechnol* 25:199–204
- Cai W, Wan J (2007) Facile synthesis of superparamagnetic magnetite nanoparticles in liquid polyols. *J Colloid Interface Sci* 305:366–370
- Cataldo F, Ursini O, Angelini G (2013) A green synthesis of colloidal silver nanoparticles and their reaction with ozone. *Eur Chem Bull* 2:700–705
- Chang YC, Kikuchi S, Kawauchi N, Sato T, Takamizawa K (2008) Complete dechlorination of tetrachloroethylene by use of an anaerobic clostridium bifermentans dph-1 and zero-valent iron. *Environ Technol* 29:381–391
- Chen Y, Wang D, Zhu X, Zheng X, Feng L (2012) Long-term Effects of copper nanoparticles on wastewater biological nutrient removal and N<sub>2</sub>O generation in the activated sludge process. *Environ Sci Technol* 46:12452–12458
- Dang F, Enomoto N, Hpio J, Enpuku K (2009) Sonochemical synthesis of monodispersed magnetite nanoparticles by using an ethanol–water mixed solvent. *Ultrason Sonochem* 16:649–654
- El-Ghandour H, Zidan HM, Khalil MMH, Ismail MIM (2012) Synthesis and some physical properties of magnetite (Fe<sub>3</sub>O<sub>4</sub>) nanoparticles. *Int J Electrochem Sci* 7:5734–5745
- El-Said WA, Yea C-H, Jung M, Kim H-C, Choi JW (2010) Analysis of effect of nanoporous alumina substrate coated with polypyrrole nanowire on cell morphology based on AFM topography. *Ultramicroscopy* 110(6):676–681
- El-Said WA, Kim T-H, Yea C-H, Kim HC, Choi JW (2011) Fabrication of gold nanoparticle modified ITO substrate to detect  $\beta$ -amyloid using surface-enhanced raman scattering. *J Nanosci Nanotechnol* 11:768–772
- El-Said WA, Cho HY, Yea CH, Choi JW (2014) Synthesis of metal nanoparticles inside living human cells based on the intracellular formation process. *Adv Mater* 26(6):910–918
- Fouad DM, Mohamed MB (2011) Studies on the photo-catalytic activity of semiconductor nanostructures and their gold core–shell on the photodegradation of malathion. *Nanotechnology* 22:455705–455713
- Fouad DM, El-Said WA, Mohamed MB (2015) Spectroscopic characterisation of magnetic Fe<sub>3</sub>O<sub>4</sub>@Au core shell nanoparticles. *Spectrochim Acta Part A Mol Biomol Spectrosc* 140:392–397
- Fouad DM, El-Said WA, Ali MH, El-Gahami MA (2017) Silica-gold nanocomposite for removal of organophosphorous pesticides. *Plasmonics* 12(3):869–875
- Jain TK, Morales MA, Sahoo SK, LesliePelecky DL, Labhassetwar V (2005) Iron oxide nanoparticles for sustained delivery of anticancer agents. *Mol Pharm* 2(3):194–205
- Jin Y, Wu M, Zhao X, (eds) (2005) Toxicity of nanomaterials to living cells. In: Technical proceedings of the 2005 NSTI nanotechnology conference and trade show
- Johannsen M, Gneveckow U, Taymoorian K, Thiesen B, Waldofner N, Scholz R, Jung K, Jordan A, Wust P, Loening SA (2007) Morbidity and quality of life during thermotherapy using magnetic nanoparticles in locally recurrent prostate cancer: results of a prospective phase I trial. *Int J Hyperther* 23:315–323
- Laurent S, Forge D, Port M, Roch A, Robic C, Elst LV, Muller RN (2008) Magnetic iron oxide nanoparticles: synthesis, stabilization, vectorization, physico-chemical characterizations and biological applications. *Chem Rev* 108(6):2064–2110
- Lu AH, Li WC, Kiefer A, Schmidt W, Bill E, Fink G, Schuth F (2004) Fabrication of magnetically separable mesostructured silica with an open pore system. *J Am Chem Soc* 126:8616–8617
- Lukman AI, Gong B, Marjo CE, Roessner U, Harris AT (2011) Facile synthesis, stabilization, and anti-bacterial performance of discrete Ag nanoparticles using *Medicago sativa* seed exudates. *Colloid Interface Sci* 353:433–444
- Maity D, Chandrasekharan P, Yang CT, Chuang KH, Shuter B, Xue JM, Ding J, Feng SS (2010) Facile synthesis of water-stable magnetite nanoparticles for clinical MRI and magnetic hyperthermia applications. *Nanomedicine* 5:1571–1584
- Modo MMI, Bulte JWM (2005) *Molecular and cellular MR imaging*. CRC Press, London
- Nunes JS, de Vasconcelos CL, Cabral FAO, de Araújo JH, Pereira MR, Fonseca JLC (2006) Synthesis and characterization of poly(ethyl methacrylate-co-methacrylic acid) magnetic particles via miniemulsion polymerization. *Polymer* 47:7646–7652
- Padil VV, Cerník M (2013) Green synthesis of copper oxide nanoparticles using gum karaya as a biotemplate and their antibacterial application. *Int J Nanomed* 8:889–898
- Parsons JG, Peralta-Videa JR, Gardea-Torresdey JL (2007) Use of plants in biotechnology: synthesis of metal nanoparticles by inactivated plant tissues, plant extracts, and living plants. *Dev Environ Sci* 5:463–485
- Prabowo B, Veriansyah B, Kim JD (2007) Supercritical water oxidation for the destruction of toxic organic wastewaters: a review. *J Environ Sci* 19:513–522
- Rockenberger J, Scher EC, Alivisatos AP (1999) A new nonhydrolytic single-precursor approach to surfactant-capped nanocrystals of transition metal oxides. *J Am Chem Soc* 121:11595–11596
- Salam HA, Rajiv P, Kamaraj M, Jagadeeswaran P, Gunalan S, Sivaraj R (2012) Plants: green route for nanoparticle synthesis. *Int J Biol Sci* 1:85–90
- Shameli K, Ahmad MB, Zamanian A, Sangpour P, Shabanzadeh P, Abdollahi Y, Zargar M (2012) Green biosynthesis of silver nanoparticles using *Curcuma longa* tuber powder. *Int J Nanomed* 7:5603–5610
- Shukla G, Kumar A, Bhandi M, Joseph PE (2006) Organochlorine pesticide contamination of ground water in the city of Hyderabad. *Environ Int* 32:244–247
- Simagina V, Likholobov V, Bergeret G, Gimenez MT, Renouprez A (2003) Catalytic hydrodechlorination of hexachlorobenzene on carbon supported Pd-Ni bimetallic catalysts. *Appl Catal B* 40:293–304
- Vishwakarma V, Samal SS, Manoharan N (2010) Safety and risk associated with nanoparticles—a review. *J Miner Mater Charact Eng* 9(05):455–459
- Wang D, Chen Y (2016) Critical review of the influences of nanoparticles on biological wastewater treatment and sludge digestion. *Crit Rev Biotechnol* 36:816–828
- Wang Y, Ma W, Chen C, Hu X, Zhao J, Yu JC (2007) Fe<sup>3+</sup>/Fe<sup>2+</sup> cycling promoted by Ta 3 N 5 under visible irradiation in Fenton degradation of organic pollutants. *Appl Catal B* 75:256–263
- Wu P, Zhu J, Xu Z (2004) Template-assisted synthesis of mesoporous magnetic nanocomposite particles. *Adv Funct Mater* 14:345–351
- Yavuz Y, Yurumez Y, Kucuker H, Ela Y, Yuksel S (2007) Two cases of acute endosulfan toxicity. *Clin Toxicol (Phila)* 45:530–532
- Zhang W, Shen F, Hong R (2011) Solvothermal synthesis of magnetic Fe<sub>3</sub>O<sub>4</sub> microparticles via self-assembly of Fe<sub>3</sub>O<sub>4</sub> nanoparticles. *Particuology* 9:179–186